

Weak ergodicity breaking of receptor motion in living cells stemming from random diffusivity

Carlo Manzo^{1,*,#}, Juan A. Torreno-Pina^{1,*}, Pietro Massignan¹, Gerald J. Lapeyre Jr.¹, Maciej Lewenstein^{1,2}, Maria F. Garcia Parajo^{1,2,#}.

¹ ICFO-Institut de Ciències Fotòniques, Mediterranean Technology Park, 08860 Castelldefels (Barcelona), Spain.

² ICREA-Institució Catalana de Recerca i Estudis Avançats, 08010 Barcelona, Spain

* Equally contributing authors.

Corresponding authors:

Carlo Manzo - ICFO-Institut de Ciències Fotòniques, Mediterranean Technology Park, 08860 Castelldefels (Barcelona), Spain - Phone: +34 935542234- E-mail: carlo.manzo@icfo.es

Maria F. Garcia-Parajo - ICFO-Institut de Ciències Fotòniques, Mediterranean Technology Park, 08860 Castelldefels (Barcelona), Spain - Phone: +34 93 5534158 - E-mail: maria.garcia-parajo@icfo.es

The recent discovery of transient immobilization as a cause of nonergodicity in the motion of some biological molecules¹⁻³ has triggered great interest for its implications in statistical mechanics and cell biology⁴⁻⁸. Is nonergodic subdiffusion a strategy shared by other biological systems? Can other physical mechanisms lead to similar behaviours? Is it beneficial? Answering to these questions is crucial to unravel the evolutionary strategy behind ergodicity breaking and its relevance for cellular function. Here we show that the motion of DC-SIGN⁹, a transmembrane receptor with unique pathogen recognition capabilities¹⁰, reveals nonergodic subdiffusion that cannot be explained by transient immobilization. Instead, its behaviour is compatible with inhomogeneity induced by spatiotemporal changes of diffusivity. The experiments are interpreted through a theoretical framework describing anomalous transport in complex media. By studying different DC-SIGN mutants, we establish a link between receptor structure and diffusivity, uncovering the relevance of nonergodicity for biological function. Our results underscore the role of spatiotemporal disorder in cell membranes, with broad implications to other heterogeneous systems where the occurrence of nonergodicity remains unexplored.

Anomalous diffusion has long been observed in a wide variety of physical systems¹¹⁻¹³. In particular, the application of single molecule techniques to living cells continues to evidence subdiffusion in the nucleus¹⁴, cytoplasm^{2,3,15,16} and in the plasma membrane^{1,17}. In subdiffusive systems^{11,12} the mean-square displacement (MSD) deviates from linearity with a scaling law $MSD \sim t^\beta$, where $\beta < 1$. Recently, analyses that go beyond MSD evaluation revealed that in some cases, subdiffusion is associated with weak ergodicity breaking¹⁻³ (wEB), with the most obvious signatures being the non-equivalence of the time-averaged MSD (MSD_t) and the ensemble-averaged MSD (MSD_{ens}), and ageing⁸, i.e., a dependence of statistical quantities on the observation time. These findings have triggered intense theoretical interest in the subject and have begun to provide insight into the physical origin of anomalous diffusion and wEB in biological systems^{4,5}. In turn, this is essential for understanding molecular mechanisms underlying cellular function, including target search¹⁸, kinetics of transport-limited reactions^{19,20}, trafficking and signalling²¹.

So far, non-ergodicity in biological systems¹⁻³ has been attributed to transient trapping and analysed within the continuous-time random walk (CTRW) framework⁶. Here we show that membrane receptors display wEB arising from mechanisms other than trapping and therefore cannot be accurately modelled by CTRW. Importantly, our experiments and theoretical model lead to a picture of wEB associated with spatiotemporal disorder. These findings are particularly relevant given that cellular components experience a highly heterogeneous environment, where the interplay of molecular crowding, diffusion barriers and specific interactions induce energetic and geometric disorder¹⁷. Moreover, our findings have broad implications to other systems in which both wEB and strong heterogeneity are the focus of current attention, but where a link between them has not been drawn yet²².

In our studies, we followed the lateral diffusion of the transmembrane pathogen-recognition receptor DC-SIGN⁹ on living cell membranes using single particle tracking²³ (SPT). DC-SIGN is involved in the binding and uptake of a broad range of pathogens¹⁰ and its spatiotemporal organization on the membrane of antigen-presenting cells plays a major role in the immunological response^{24,25}. We recorded the mobility of quantum-dot labelled wild type (wt)DC-SIGN transfected in Chinese Hamster Ovary (CHO) cells^{24,25} (Fig. 1a-b). The MSD_t of individual trajectories displayed a linear behaviour, consistent with pure Brownian diffusion (Fig. 1c). We then calculated the diffusion coefficient D_s for each trajectory by a linear fit of the MSD_t at short-time lags²⁶. The resulting values of D_s were highly heterogeneous, spanning more than two orders of magnitude (Fig. 1d). Interestingly, the MSD_{ens} deviated significantly from linearity, showing subdiffusion with exponent $\beta=0.84\pm 0.03$ (Fig. 1e). These results show a different scaling of MSD_t and MSD_{ens} , revealing a clear signature of wEB⁶. To enquire whether DC-SIGN dynamics also exhibits ageing, we computed the time-ensemble-averaged MSD ($\text{MSD}_{t,\text{ens}}$) by truncating the data at different observation times T , and extracting the corresponding diffusion coefficient $D_{t,\text{ens}}$ by linear fitting²⁶. Under rather general assumptions^{7,27} it can be shown that $D_{t,\text{ens}} \sim T^{\beta-1}$. $D_{t,\text{ens}}$ scaled as a power law with an exponent of -0.17 ± 0.05 (Fig. 1f), yielding a value of β that is in good agreement with the exponent determined from MSD_{ens} . These results demonstrate that wtDC-SIGN dynamics exhibits ageing.

wEB and ageing due to energetic disorder and transient trapping are well described by a CTRW model with infinite mean waiting-time⁵⁻⁷. To compare DC-SIGN diffusion to the CTRW predictions, we searched for the occurrence of transient immobilization events on individual trajectories. Surprisingly, transient immobilization was only detected in less than 5% of the total recording time (Fig. 2a-c) and trapping times followed an exponential decay with average duration of 330 ± 30 ms (Fig. 2d). Moreover, we constructed the distribution of escape times by identifying the duration of the events in which a trajectory remains within a given radius R_{TH} (Fig. 2e), which for CTRW is expected to be independent on R_{TH} (ref. 1). In strong contrast, escape-time distributions of DC-SIGN trajectories showed a marked dependence on R_{TH} (Fig. 2f). The sporadic occurrence of transient trapping events, the lack of long immobilization times, their exponential distribution, and the dependence of escape-time distributions on R_{TH} are all inconsistent with CTRW, indicating that this model fails to explain DC-SIGN dynamics.

To address the origin of the observed DC-SIGN nonergodic behaviour, we further analysed individual trajectories by means of a change-point algorithm to detect variations of diffusivity in time²⁸. Notably, DC-SIGN trajectories displayed a Brownian motion with relatively constant diffusivity over intervals of varying length, but that changed significantly between these intervals (Fig. 3a-c). Similar features were identified in a large fraction of trajectories, with $\sim 63\%$ showing at least one diffusivity change (Fig. 3d). These results qualitatively agree with a class of models we recently proposed, describing ordinary Brownian motion with a diffusivity that varies randomly, but is constant on time intervals or spatial patches with random size²⁷. These models describe anomalous diffusion

and wEB in complex and heterogeneous media, such as the cellular environment, without invoking transient trapping.

To obtain a comprehensive understanding of our data, we considered an annealed model²⁷ which assumes that randomly diffusing particles undergo sudden changes of diffusion coefficient. The distribution of diffusion coefficients D that a particle can experience is assumed to have a power-law behaviour $\sim D^{\sigma-1}$ for small D (with $\sigma > 0$) and a fast decay for $D \rightarrow \infty$. Given D , the transit time τ (i.e., the time τ a particle dwells with a given D) is taken to have a probability distribution with mean $\sim D^{-\gamma}$. Depending on the relative values of the exponents σ and γ , this model predicts three different regimes²⁷, namely: (0) for $\gamma < \sigma$, the overall dynamics is compatible with ordinary Brownian motion and yields an MSD exponent $\beta=1$; (I) for $\sigma < \gamma < \sigma+1$, the average transit time diverges and particles undergo nonergodic subdiffusion with $\beta=\sigma/\gamma$; (II) for $\gamma > \sigma+1$, the averages of both the transit time and the explored area diverge and one obtains nonergodic subdiffusion with $\beta=1-1/\gamma$.

We performed *in-silico* experiments of 2D diffusion (Fig. 4a-b), assuming a distribution of diffusion coefficients given by:

$$P_D(D) = \frac{D^{\sigma-1} e^{-D/b}}{b^\sigma \Gamma(\sigma)}, \quad (1)$$

and a conditional distribution of transit times τ given by:

$$P_\tau(\tau|D) = \frac{D^\gamma}{k} e^{-\tau D^\gamma/k}, \quad (2)$$

where b and k are dimensional constants and $\Gamma(x)$ is the Gamma function. We performed simulations for different σ , with $\gamma = \sigma/\beta$ as in regime (I) and $\beta=0.84$, the exponent obtained from MSD_{ens} . The simulations quantitatively reproduce not only subdiffusion, nonergodicity and ageing, but also the heterogeneous distribution of diffusion coefficients and escape time distributions (Fig. 4c-h). The remarkable agreement between simulations and experimental data strongly supports heterogeneous diffusion as the origin for DC-SIGN nonergodicity.

To gain insight into the molecular mechanisms of DC-SIGN nonergodic diffusion, we extended the analysis and simulations to three mutated forms of the receptor (Fig. 5a). These mutations have been reported to affect the interaction of DC-SIGN with other cellular components, strongly affecting DC-SIGN function^{24,25,29}. The N80A presents a point mutation within the N-glycosylation motif hindering glycan-based interactions with components of the extracellular membrane²⁵. The $\Delta 35$ lacks the first 35 amino acids from the N terminus in the cytoplasmic tail, preventing interactions with cytosolic components such as actin²⁹. Finally, the ΔRep lacks the tandem repeats in the extracellular neck region abrogating DC-SIGN homo-interactions²⁴.

We found that each mutation has a very different effect on the dynamics of the receptor. Both N80A (Fig. 5c-f) and $\Delta 35$ (Fig. 5g-l) showed nonergodic dynamics similar to that observed for wtDC-SIGN, while ΔRep dynamics yielded ergodic

Brownian diffusion (Fig. 5m-p). Moreover, the extent of heterogeneity in the diffusion coefficients of $\Delta 35$ is similar to that of wtDC-SIGN (Fig. 5i), but is larger in the case of N80A (Fig. 5e) and is highly reduced on Δ Rep (Fig. 5o). We accurately reproduced N80A and $\Delta 35$ dynamics by simulations performed in regime (I), i.e., nonergodic subdiffusion, using comparable values of γ for wtDC-SIGN and $\Delta 35$, and a smaller value of γ for N80A (Fig. 5b). In contrast, the behaviour of Δ Rep was fully captured by *in-silico* experiments in regime (0), i.e., ordinary Brownian motion.

What is the relevance of nonergodicity for DC-SIGN biological function? At the structural level, wtDC-SIGN, N80A and $\Delta 35$ preferentially form nanoclusters, which are thought to regulate pathogen binding^{24,25}, whereas deletion of the tandem repeat (Δ Rep) reduces nanoclustering and binding efficiency²⁴. Our results thus show that the diffusive behaviour of the receptor is strongly linked to nanoclustering. Given that the plasma membrane is highly heterogeneous, our data indicate that nonergodicity stems from the ability of DC-SIGN nanoclusters to interact with the membrane environment, including components from the outer and inner membrane leaflet. This interaction is absent in the Δ Rep mutant since it does not form nanoclusters. In further support of this evidence, we observed that both wtDC-SIGN and N80A exhibited nonergodicity, although N80A diffusivity is significantly more heterogeneous than for wtDC-SIGN. This increased heterogeneity correlates with altered interactions of the N80A with extracellular components, resulting from the deletion of the glycosylation motif²⁵. Thus, it appears that the extracellular milieu next to the membrane contributes to the degree of dynamical heterogeneity sensed by the receptor. Remarkably, this correlation also extends to the functional level, as we recently showed that interactions with extracellular glycan-binding proteins influence clathrin-mediated encounters with DC-SIGN and endocytosis²⁵. In contrast, $\Delta 35$ and wtDC-SIGN exhibit similar nanoclustering²⁴, nonergodicity and diffusion heterogeneity, albeit $\Delta 35$ is not able to interact with cytosolic components in close proximity to the inner membrane, including actin²⁹. Therefore, in contrast to the extracellular influence, these results interestingly show that interactions with the actin cytoskeleton, responsible for the CTRW-like behaviour of other proteins¹, do not play a role in DC-SIGN dynamics.

In summary, we demonstrated that DC-SIGN displays nonergodic subdiffusive dynamics. In contrast to other biological systems, this behaviour may not be ascribed to transient immobilization and therefore cannot be explained in terms of CTRW. DC-SIGN dynamics is instead accurately described using a model of ordinary random walk with spatiotemporal heterogeneity of diffusivity. Comparative analysis of mutated forms of the receptor allowed us to establish the relevance of nonergodicity for the mechanisms regulating receptor capacity for pathogen recognition and internalization. The evidence that spatiotemporal disorder induces subdiffusion and wEB provides a novel and more realistic framework for interpreting anomalous motion in cell membranes given their highly heterogeneous character, as well as being applicable to other biological processes and complex media.

Methods

Cell culture and labelling

Chinese hamster ovary (CHO) cells stably transfected with DC-SIGN mutants were cultured in HAM's F-12 medium (LabClinics) supplemented with 10% fetal calf serum and antibiotic/antimycotic (Gibco). CHO cells were seeded onto 25 mm coverslips 24 hours before imaging. Streptavidin-coated quantum dots (Qdot655, Invitrogen) were added to an equimolar solution of biotinylated anti-DC-SIGN DCN46 Fab fragment (or anti-AU1 monovalent Ab, in the case of Δ Rep mutant) and a 50x excess of free biotin (Gibco) in order to obtain a 1:1 Fab fragment-quantum dot ratio (or monovalent Ab-quantum dot ratio, in the case of Δ Rep mutant). After at least 2 h at 4°C, cells were incubated with 50 pM conjugated quantum dots for 5 min at RT. Extensive washing was performed to remove non-bound conjugated quantum dots before imaging. Fab fragments and monovalent Ab were obtained as described in refs. ^{24,25}.

Single particle tracking experiments

We performed video microscopy using a custom single-molecule sensitive epifluorescence microscope. Continuous excitation was provided by the 488-nm line of an Argon-ion laser (Spectra Physics), with power density at the sample plane of ~ 0.3 kW/cm². Fluorescence was collected by means of a 1.2 NA water immersion objective (Olympus) and guided into an intensified EM-CCD camera (Hamamatsu) after suitable filtering. Movies were recorded on the dorsal membrane of CHO cells at 60Hz frame rate. Experiments were performed at 37 °C and in 5% CO₂ atmosphere. Trajectories were analysed with custom Matlab code based on the algorithm described in ref. 30. To avoid false-positive reconnection, trajectories were overlaid to raw movies and visually inspected.

Data analysis

Time-, ensemble- and time-ensemble-averaged mean-squared displacements were calculated as described in ref. 1. Exponents of the MSD_{ens} and $D_{t,ens}$ were obtained by linear fitting of the log-log transformed data. Errors were calculated as the 99% confidence interval of the fitting parameters. Short-time diffusion coefficients were extracted from the linear fit of the first 10% of the points of MSD_t curves²⁶.

Measurements of the apparent diffusion of quantum dots on fixed cells and glass coverslips were used to estimate the smallest detectable diffusivity. Short-time diffusion coefficients were obtained as described above for trajectories of immobilized quantum dots and the corresponding probability distribution was calculated. 95% of the immobilized quantum dots trajectories showed values lower than $6 \cdot 10^{-4}$ $\mu\text{m}^2/\text{s}$, which was therefore set as the threshold (D_{TH}) for classifying a trajectory as mobile.

Dynamical changes in the motion of DC-SIGN receptors were identified by application of the change-point algorithm described in ref. 28. In brief, the trajectories were recursively segmented and a maximum-likelihood-ratio test

was applied to the trajectory displacements (Δx , Δy) in order to identify sudden changes of diffusivity. The critical values for Type I error rates were set to a confidence level of 99%, corresponding to 1% probability of having a false-positive identification of a change-point. For each dynamical region identified by the algorithm, the short-time diffusion coefficient was calculated from a linear fit of the first 10% of the points of the corresponding MSD curves²⁶. Regions showing a short-time diffusion coefficient lower than D_{TH} were considered compatible with transient immobilization.

Simulations

Simulated trajectories (500 per parameter set) were obtained by generating random diffusion coefficients D according to the probability distribution given in (1). For each diffusion coefficient, the corresponding transit time τ was calculated as a random number drawn from the distribution given in (2). Particle coordinates were generated as:

$$\begin{aligned}x_{t+\Delta t'} &= x_t + \sqrt{2D\Delta t'} \xi_x \\y_{t+\Delta t'} &= y_t + \sqrt{2D\Delta t'} \xi_y,\end{aligned}$$

where $\xi_{x,y}$ are random numbers from a Gaussian distribution with zero mean and unitary standard deviation. The time increment was calculated as $\Delta t' = \Delta t/n$, where Δt is the camera acquisition rate and n is a integer depending on D and τ , in order to have at least 10 points for each interval. For comparison with SPT data, trajectories were sub-sampled at the camera acquisition rate and cut to the same length as the experimental trajectories, starting from a randomly generated initial time. Gaussian noise corresponding to the experimental localization accuracy ($\sigma_{acc} = 20$ nm) was subsequently added to the trajectories.

References

- 1 Weigel, A. V., Simon, B., Tamkun, M. M. & Krapf, D. Ergodic and nonergodic processes coexist in the plasma membrane as observed by single-molecule tracking. *Proc. Natl. Acad. Sci. U. S. A.* **108**, 6438-6443, (2011).
- 2 Jeon, J.-H. *et al.* In Vivo Anomalous Diffusion and Weak Ergodicity Breaking of Lipid Granules. *Phys. Rev. Lett.* **106**, 048103, (2011).
- 3 Tabei, S. M. A. *et al.* Intracellular transport of insulin granules is a subordinated random walk. *Proc. Natl. Acad. Sci. U. S. A.* **110**, 4911-4916, (2013).
- 4 Cherstvy, A. G., Chechkin, A. V. & Metzler, R. Anomalous diffusion and ergodicity breaking in heterogeneous diffusion processes. *New J. Phys.* **15**, 083039, (2013).
- 5 Barkai, E., Garini, Y. & Metzler, R. Strange kinetics of single molecules in living cells. *Phys. Today* **65**, 29-29, (2012).
- 6 Bel, G. & Barkai, E. Weak Ergodicity Breaking in the Continuous-Time Random Walk. *Phys. Rev. Lett.* **94**, 240602, (2005).
- 7 Lubelski, A., Sokolov, I. M. & Klafter, J. Nonergodicity Mimics Inhomogeneity in Single Particle Tracking. *Phys. Rev. Lett.* **100**, 250602, (2008).

- 8 Barkai, E. Aging in Subdiffusion Generated by a Deterministic Dynamical System. *Phys. Rev. Lett.* **90**, 104101, (2003).
- 9 Geijtenbeek, T. B. H. *et al.* DC-SIGN, a Dendritic Cell-Specific HIV-1-Binding Protein that Enhances trans-Infection of T Cells. *Cell* **100**, 587-597, (2000).
- 10 van Kooyk, Y. & Geijtenbeek, T. B. H. DC-SIGN: escape mechanism for pathogens. *Nat. Rev. Immunol.* **3**, 697-709, (2003).
- 11 Havlin, S. & Ben-Avraham, D. Diffusion in disordered media. *Adv. Phys.* **36**, 695-798, (1987).
- 12 Bouchaud, J.-P. & Georges, A. Anomalous diffusion in disordered media: Statistical mechanisms, models and physical applications. *Phys. Rep.* **195**, 127-293, (1990).
- 13 Felix, H. & Thomas, F. Anomalous transport in the crowded world of biological cells. *Rep. Prog. Phys.* **76**, 046602, (2013).
- 14 Bronstein, I. *et al.* Transient Anomalous Diffusion of Telomeres in the Nucleus of Mammalian Cells. *Phys. Rev. Lett.* **103**, 018102, (2009).
- 15 Weiss, M., Elsner, M., Kartberg, F. & Nilsson, T. Anomalous Subdiffusion Is a Measure for Cytoplasmic Crowding in Living Cells. *Biophys. J.* **87**, 3518-3524, (2004).
- 16 Golding, I. & Cox, E. C. Physical Nature of Bacterial Cytoplasm. *Phys. Rev. Lett.* **96**, 098102, (2006).
- 17 Saxton, M. J. & Jacobson, K. Single-particle tracking: applications to membrane dynamics. *Annu. Rev. Biophys. Biomol. Struct.* **26**, 373-399, (1997).
- 18 Condamin, S., Benichou, O., Tejedor, V., Voituriez, R. & Klafter, J. First-passage times in complex scale-invariant media. *Nature* **450**, 77-80, (2007).
- 19 Lomholt, M. A., Zaid, I. M. & Metzler, R. Subdiffusion and Weak Ergodicity Breaking in the Presence of a Reactive Boundary. *Phys. Rev. Lett.* **98**, 200603, (2007).
- 20 Condamin, S., Tejedor, V., Voituriez, R., Bénichou, O. & Klafter, J. Probing microscopic origins of confined subdiffusion by first-passage observables. *Proc. Natl. Acad. Sci. U. S. A.* **105**, 5675-5680, (2008).
- 21 Choquet, D. & Triller, A. The role of receptor diffusion in the organization of the postsynaptic membrane. *Nat. Rev. Neurosci.* **4**, 251-265, (2003).
- 22 Berkowitz, B., Cortis, A., Dentz, M. & Scher, H. Modeling non-Fickian transport in geological formations as a continuous time random walk. *Rev Geophys* **44**, (2006).
- 23 Kusumi, A., Tsunoyama, T. A., Hirose, K. M., Kasai, R. S. & Fujiwara, T. K. Tracking single molecules at work in living cells. *Nat. Chem. Biol.* **10**, 524-532, (2014).
- 24 Manzo, C. *et al.* The neck region of the C-type lectin DC-SIGN regulates its surface spatiotemporal organization and virus-binding capacity on antigen-presenting cells. *J. Biol. Chem.* **287**, 38946-38955, (2012).
- 25 Torreno-Pina, J. A. *et al.* Enhanced receptor-clathrin interactions induced by N-glycan mediated membrane micropatterning. *Proc. Natl. Acad. Sci. U. S. A.*, in press, (2014).

- 26 Michalet, X. Mean square displacement analysis of single-particle trajectories with localization error: Brownian motion in an isotropic medium. *Physical Review E* **82**, 041914, (2010).
- 27 Massignan, P. *et al.* Nonergodic Subdiffusion from Brownian Motion in an Inhomogeneous Medium. *Phys. Rev. Lett.* **112**, 150603, (2014).
- 28 Montiel, D., Cang, H. & Yang, H. Quantitative characterization of changes in dynamical behavior for single-particle tracking studies. *J. Phys. Chem. B* **110**, 19763-19770, (2006).
- 29 Smith, A. L. *et al.* Leukocyte-specific protein 1 interacts with DC-SIGN and mediates transport of HIV to the proteasome in dendritic cells. *J. Exp. Med.* **204**, 421-430, (2007).
- 30 Sergé, A., Bertaux, N., Rigneault, H. & Marguet, D. Dynamic multiple-target tracing to probe spatiotemporal cartography of cell membranes. *Nat. Methods* **5**, 687-694, (2008).

Acknowledgements

We thank A. Cambi for providing DC-SIGN transfected CHO cells, O. Esteban for preparing the Fab fragments, P. Symeonidou Besi for preliminary data analysis and B. Castro for carrying out N80A experiments. This work was supported by Fundació Cellex, Generalitat de Catalunya (Grant No. 2009 SGR 597), the European Commission (FP7-ICT-2011-7, Grant No. 288263), the HFSP (Grant No. RGP0027/2012), ERC AdG Osyris, and the Spanish Ministry of Science and Innovation (Grants No. FIS2008-00784 and No. MAT2011-22887).

Author Contributions

C.M. analysed the data and performed the simulations. J.A.T.-P. performed the experiments and the data processing. G.J.L. and P.M. developed the theoretical model. M.L. and M.F.G.-P. supervised the project. All authors contributed to numerous discussions and wrote the paper.

Figures

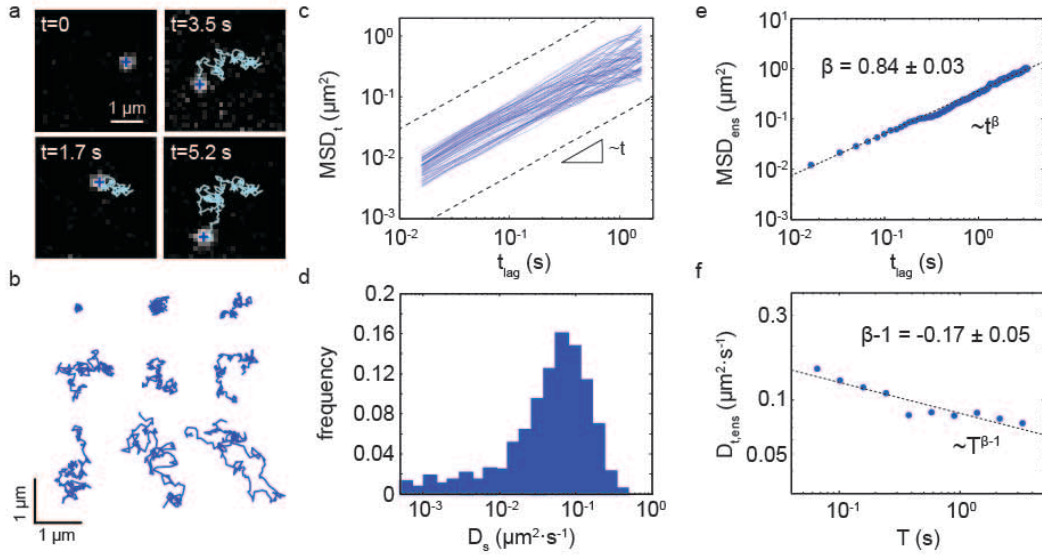


Figure 1 | DC-SIGN diffusion shows weak ergodicity breaking and ageing.

(a) Representative video frames of a quantum-dot-labelled wtDC-SIGN molecule diffusing on the dorsal membrane of a CHO cell. The centroid position of the bright spot (+), corresponding to a single quantum-dot, is tracked and reconnected to build up the DC-SIGN trajectory, shown by the cyan line. (b) Representative trajectories of wtDC-SIGN for the same recording time (3.2 s). (c) Log-log plot of the time-averaged MSD for representative wtDC-SIGN trajectories (blue lines). The dashed lines scale linearly in time, showing that MSD_t is compatible with pure Brownian motion ($\beta=1$). (d) Distribution of short-time diffusion coefficients as obtained from linear fitting of the time-averaged MSD for all the DC-SIGN trajectories. (e) Log-log plot of the ensemble-averaged MSD. Power law fit of the data (dashed line) provided exponent $\beta=0.84$, showing subdiffusion. (f) Log-log plot of the time-ensemble-averaged diffusion coefficient as a function of the observation time T . The diffusion coefficients are obtained by linear fitting of the time-ensemble-averaged MSD. A power-law fit (dashed line) provides an exponent $\beta-1=-0.17$, revealing ageing.

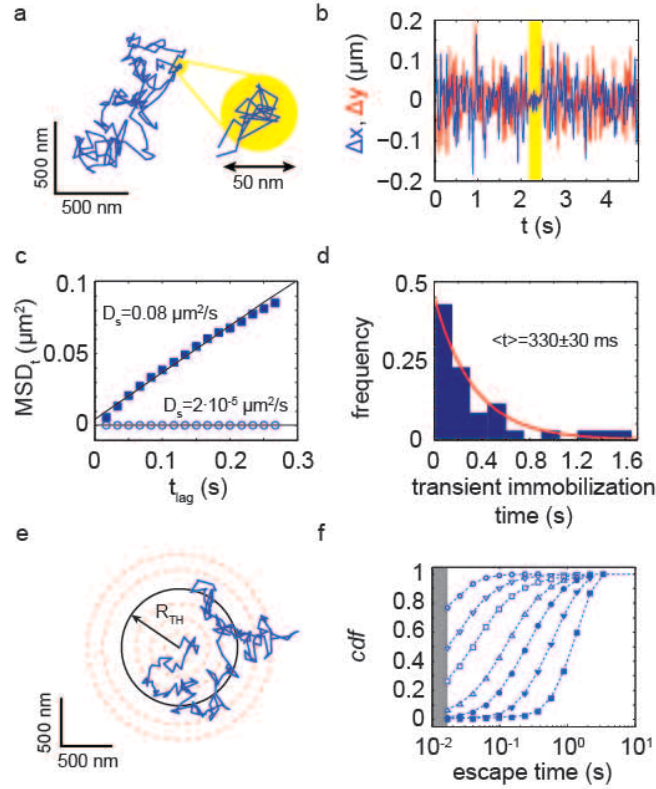


Figure 2 | DC-SIGN receptor dynamics is inconsistent with the CTRW model.

(a) A trajectory of wtDC-SIGN on living cell showing short-lived transient immobilization event, highlighted by the yellow circular area. (b) Plot of the x- (blue) and y-displacement (red) as a function of time. The occurrence of transient immobilization (yellow region) corresponds to a reduction in the trajectory displacement. (c) Time-averaged MSD for the entire trajectory (■) and for the immobilization region only (○). (d) Histogram of the duration of the immobilization events for wtDC-SIGN trajectories. The distribution shows an exponential decay with an average immobilization time of 330 ± 30 ms. The total duration of the immobilization events observed in all the wtDCSIGN trajectories accounts for $\sim 5\%$ of the total recording time. (e) Schematic representation of the calculation of the escape time probability from circular areas of different radius R_{TH} . (f) Cumulative probability distribution function (*cdf*) of trajectory escape time for different radii $R_{TH} = 20$ nm (○), 50 nm (▽), 100 nm (□), 200 nm (△), 300 nm (●), 500 nm (▼) and to 1000 nm (■). Dashed lines are guides to the eye. The grey shaded region represents times shorter than the acquisition frame rate.

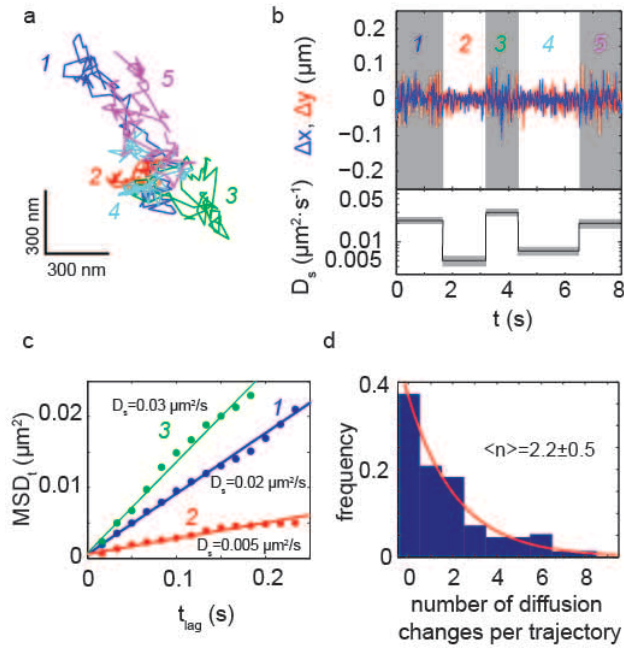


Figure 3 | DC-SIGN motion experiences changes in diffusivity. (a) Representative wtDC-SIGN trajectory displaying changes of diffusivity. Change-point analysis evidenced 5 different regions represented with different colours. (b) Plot of the x- (blue) and y-displacement (red) for the DC-SIGN trajectory in (a) as a function of time. The shaded areas indicate the regions of different diffusivity. The lower panel displays the corresponding short-time diffusion coefficient as obtained from a linear fit of the time-averaged MSD for the 5 different regions. Grey areas correspond to the 95% confidence level. (c) Plot of time-averaged MSD versus time lag for the first three regions of the trajectory in (a). (d) Histogram of the number of changes of diffusion per trajectory. Most of the trajectories (63%) display at least one dynamical change, with an average of 2.2 changes per trajectory.

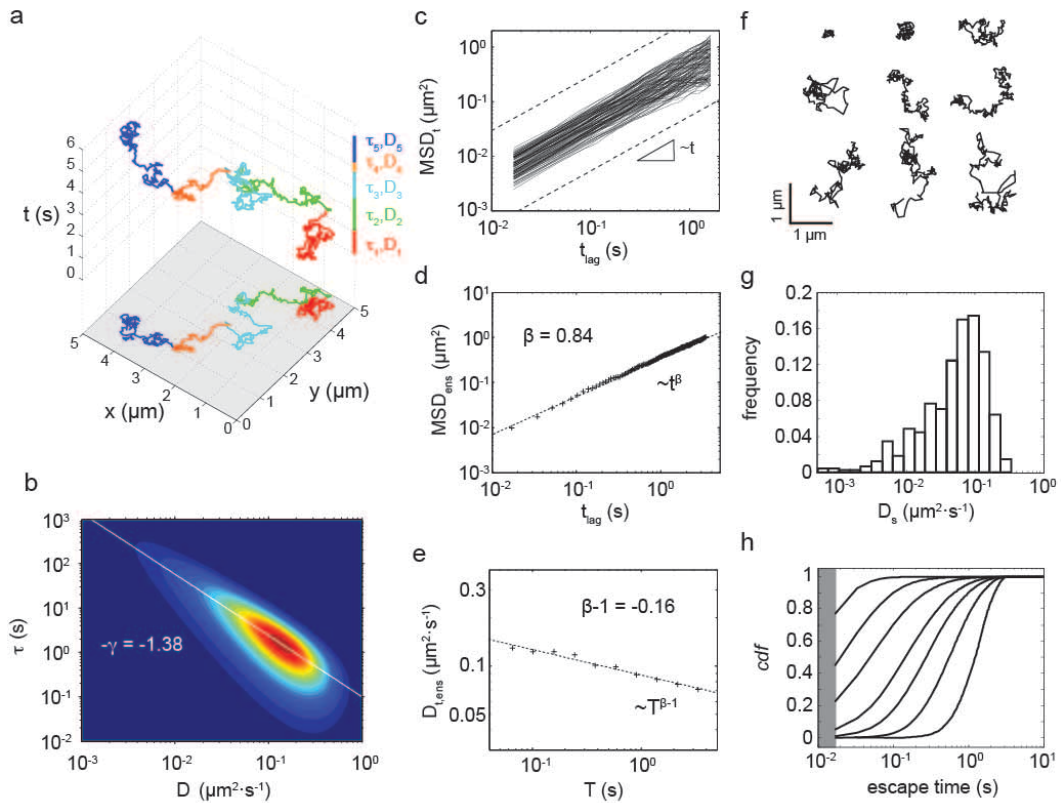


Figure 4 | Annealed model of heterogeneous diffusion quantitatively reproduces DC-SIGN motion. (a) Three-dimensional plot of a simulated trajectory composed by five time intervals with different transit time τ_i and diffusivity D_i . (b) Contour plot of the normalized distribution of the simulated diffusion coefficient (D) and transit time (τ) for the parameters reproducing the dynamics of wtDC-SIGN ($\sigma=1.16$, $\gamma=1.38$, $b=0.12 \mu\text{m}^2\cdot\text{s}^{-1}$, $k=0.10 \mu\text{m}^{2\gamma}\cdot\text{s}^{\gamma+1}$). The white line represents the power law dependence between diffusivity and average transit time with exponent $-\gamma$. (c) Log-log plot of the time-averaged MSD for representative simulated trajectories (black lines). (d) Log-log plot of the ensemble-averaged MSD for the simulated trajectories. The dashed line represents a power law with the theoretical exponent $\beta=\sigma/\gamma=0.84$. (e) Log-log plot of the time-ensemble averaged diffusion coefficient as a function of the observation time T . The dashed line represents a power law with the theoretical exponent $\beta-1=-0.16$. (f) Representative simulated trajectories for the same recording time (3.2 s). (g) Distribution of short-time diffusion coefficients as obtained from linear fitting of the time-averaged MSD for all the simulated trajectories. (h) *cdf* of trajectory escape time for different radii. Curves from left to right correspond to radii $R_{\text{TH}}=20$ nm, 50 nm, 100 nm, 200 nm, 300 nm, 500 nm and to 1000 nm.

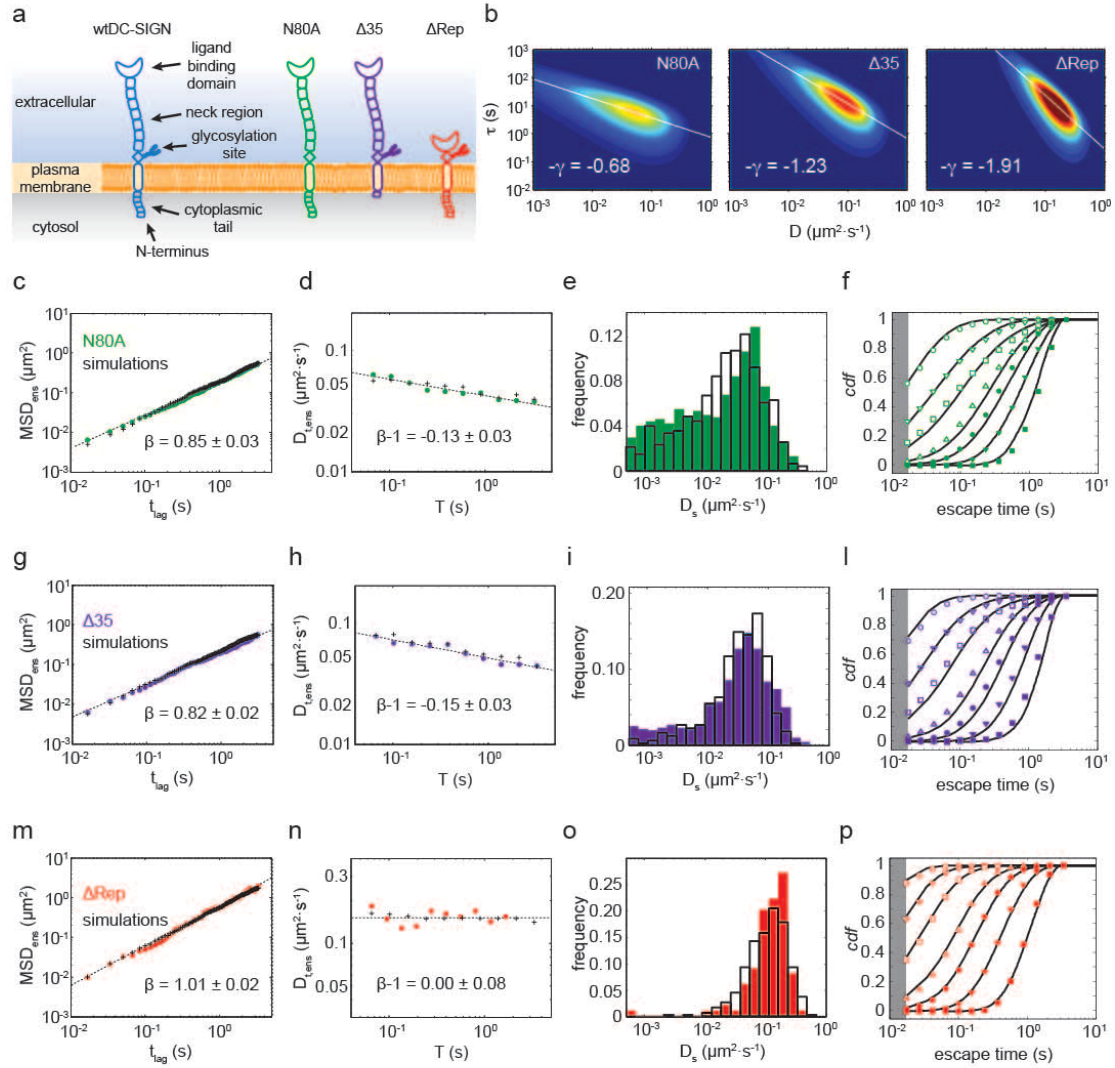


Figure 5 | Effect of mutations on the dynamics of DC-SIGN. (a) Schematic representation of wtDC-SIGN and its mutated forms. (b) Contour plot of the normalized distribution of the simulated diffusion coefficient (D) and transit time (τ) for the parameters reproducing the dynamics of N80A ($\sigma=0.58$, $\gamma=0.68$, $b=0.09 \mu\text{m}^2\cdot\text{s}^{-1}$, $k=0.74 \mu\text{m}^{2\gamma}\cdot\text{s}^{\gamma+1}$), $\Delta 35$ ($\sigma=1.04$, $\gamma=1.23$, $b=0.08 \mu\text{m}^2\cdot\text{s}^{-1}$, $k=0.07 \mu\text{m}^{2\gamma}\cdot\text{s}^{\gamma+1}$) and ΔRep ($\sigma=2.11$, $\gamma=1.91$, $b=0.07 \mu\text{m}^2\cdot\text{s}^{-1}$, $k=0.07 \mu\text{m}^{2\gamma}\cdot\text{s}^{\gamma+1}$). The white line represents the power law dependence between diffusivity and average transit time with exponent $-\gamma$. (c) Log-log plot of the ensemble-averaged MSD for N80A trajectories (\bullet) and simulated data (+). (d) Log-log plot of the time-ensemble averaged diffusion coefficient for N80A trajectories (\bullet) and simulated data (+) as a function of the observation time T . (e) Distribution of short-time diffusion coefficients as obtained from linear fitting of the time-averaged MSD for the N80A (filled bars) and the simulated trajectories (empty bars). (f) *cdf* of the escape time for N80A (symbols) and simulated trajectories (lines) for different radii. The meaning of the symbols is the same as in Fig. 2f. (g-l) Dynamical behaviour of the $\Delta 35$ mutant. (m-p) Dynamical behaviour of the ΔRep mutant.